Supporting Information

Structure and Thermochemistry of Perrhenate Sodalite and Mixed Guest Perrhenate/Pertechnetate Sodalite

Eric M. Pierce[a‡*], Kristina Lilova[b‡], David M. Missimer[c], Wayne W. Lukens[d], Lili Wu[b], Jeffrey Fitts[e], Claudia Rawn[f], Ashfia Huq[g], Donovan N. Leonard[f], Jeremy R. Eskelsen[a], Brian F. Woodfield[h], Carol M. Jantzen[i], and Alexandra Navrotsky[b]

[a]Environmental Sciences Division, Oak Ridge National Laboratory, P.O. Box 2008, MS: 6038, Oak Ridge, TN 37831

[b]Peter A. Rock Thermochemistry Laboratory and NEAT ORU, University of California at Davis, Davis, CA 95616

[c]Analytical Development Center, Savannah River National Laboratory, Aiken, SC 29808

[d]Chemical Sciences Division, Lawrence Berkeley National Laboratory, Berkeley, CA 94720

[e]Department of Civil & Environmental Engineering, Princeton University, Princeton, NJ 08544

[f]Department of Materials Science & Engineering, University of Tennessee, Knoxville, TN 37996

[g]Chemical & Engineering Materials Division, Oak Ridge National Laboratory, P.O. Box 2008, Oak Ridge, TN 37831

[h]Chemistry & Biochemistry, Brigham Young University, Provo, UT 84602

[i]Environmental Technology Center, Savannah River National Laboratory, Aiken, SC 29808

Synthesis and Characterization Methods and Materials. Crystalline perrhenate sodalite, $Na_8[AlSiO_4]_6(ReO_4)_2$, was prepared by reacting Zeolite 4A—also referred to as molecular sieve 4A—with 8M NaOH in the presence of excess sodium perrhenate ($NaReO_4$) at 225°C and 400 psi in an autoclave for 7 d. Zeolite 4A has a chemical composition of $Na_2O•Al_2O_3•2SiO_2•9/2H_2O$ and a SiO_2/Al_2O_3 ratio of approximately two. The hydrothermal synthesis was carried out in a Teflon-lined Parr pressure vessel. The Teflon liners were filled with 0.004 mol Zeolite 4A as a precursor, 0.29 mol $NaReO_4$, and 110 mL of 8M NaOH. After reacting for 7 d at 225°C in a constant temperature oven, the solid slurry was removed and centrifuged, washed and centrifuged several times, and dried overnight at 105°C. The bulk sample was synthesized in small batches (i.e., ~7 to 12 grams material was produced per batch). Each batch was combined into a single container and then mixed on a shaker to produce 200 grams homogenized material. Surface area and particle size of the homogenized sample were determined with a Micromeritics ASAP 2020 (N_2-adsorption BET surface area) and a Microtrac S3500 particle size analyzer, respectively.

Crystalline mixed guest perrhenate/pertechnetate sodalite, $Na_8[AlSiO_4]_6(ReO_4)_{2-x}(TcO_4)_x$, was prepared hydrothermally using a similar synthesis approach described for $Na_8[AlSiO_4]_6(ReO_4)_2$. The Teflon liner was filled with 0.00032 mol of the precursor Zeolite 4A, 0.021 mol of $NaReO_4$, 0.0019 mol of $NaTcO_4$, and 8.57 mL of 8M NaOH. After reacting for 8 d at 225°C in a constant temperature oven, the slurry was removed and washed using a microanalysis vacuum filter assembly with a 0.5 mm Millipore Teflon filter. The solids were washed with deionized water until the wash solution pH dropped between 7 and 8, and then the solids were dried at 105°C overnight. The amount of material synthesized was 0.68 grams. Crystal structure of the resulting mixed guest perrhenate/pertechnecate sodalite was analyzed on a Bruker D8 XRD using CuKα

radiation source. The $NaTcO_4$ used in the synthesis was produced by reacting 0.34 grams of NH_4TcO_4 with 1.41 mL of 0.9M NaOH and 4.26 mL of deionized water in a Teflon liner. The resulting $NaTcO_4$ solid was dried in a constant temperature oven for 24 hours at 105°C and cooled to room temperature before use.

Scanning electron (SEM) images of perrhenate sodalite and mixed perrhenate/pertechnetate sodalite powder was performed using an electron beam of a Hitachi NB-5000 FIB/SEM and a Zeiss Sigma VP Field-Emission SEM, respectively. The as-received material was dispersed on an aluminum stub coated with carbon tape. A Cressington 208HR sputter coater, equipped with a thickness monitor, was used to deposit ~10 nm of platinum/palladium metal onto the powder sample to reduce charging under the electron beam during SEM imaging. The SEM secondary electron micrographs were acquired at 5kV with normal probe current and a working distance of 4.9 mm.

In addition to aforementioned characterization measurements, chemical composition was measured using a combination of electron microanalysis, chemical digestion, Fourier transform infrared (FTIR), and thermogravimetric analysis. The electron microanalysis was conducted to verify the homogeneity and stoichiometry of the samples using a Cameca SX-100 electron microprobe with the following conditions: HV of 15 kV, beam current of 2 nA, and beam size of 5 μm. The homogenized sample also was chemically digested with an alkaline fusion, and the composition of the resulting solutions was analyzed with inductively coupled optical emission spectroscopy and/or inductively coupled plasma mass spectrometry. A Bruker Equinox 55 FTIR spectrometer was used to determine the presence of both structural and adsorbed surface water.

Two types of thermogravimetric (TG)/differential scanning calorimetry (DSC) (Setaram Labsys Evo) measurements were performed in the temperature range from 973 to 1,273 K.[1] The first type of TG/DSC measurement consisted of annealing an aliquot of the perrhenate sodalite sample in an empty Pt crucible, whereas the second consisted of dissolving the sample in molten lead borate. Dissolution of the perrhenate sodalite was accompanied by water vapor leaving the melt. In both cases, the initial and final weights were measured to determine any weight loss related to the water content or other possible reactions.

Chemical Composition, Particle Size, and Surface Area of Perrhenate Sodalite Results. The electron probe microanalysis and chemical digestion analyses results are provided in Table S1. The aluminum, sodium, and silicon content of the sample prepared in this study is comparable to the theoretical composition and the sample prepared by Mattigod et al. [2] (see Table S1). Unlike the other elements, the rhenium content for the sample prepared in this study is much closer to the theoretical composition in comparison with the sample prepared by Mattigod et al. [2] (30.6 ±1.2 wt % rhenium), which had ~4 wt % higher rhenium.

The size of the perrhenate sodalite ranged from 0.5 to 5 μm for individual particles and <10 μm for aggregates based on SEM and laser diffraction particle size analyses, respectively (Fig. S1). The N_2-BET surface area was 3.09(2) m^2/g. Both measurements, particle size and surface area, are consistent with previous results.[2] The absence of the adsorption band at 1,630 cm^{-1} (assigned to molecular water) and 3,500 cm^{-1} (assigned to H_2O and/or OH groups) in the FTIR spectra confirmed the absence of molecular water. This also was confirmed by both of the thermogravimetry in solvent analysis techniques, which did not register weight change in either case.

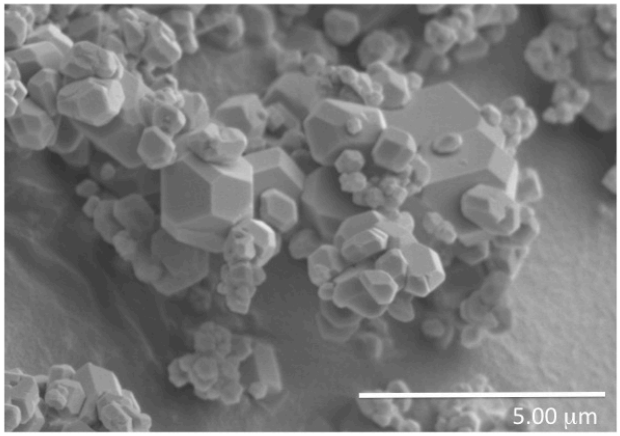

Figure SI1. Scanning electron microscope image of dispersed and agglomerated perrhenate sodalite particles. Image illustrates the variation in particle size from 0.5 to 5 µm and <10 µm for dispersed and agglomerated particles, respectively.

Table SI1. Chemical composition (mass%)

Element	Stoichiometric Composition	Microprobe	Chemical Digestion	This Study[a]	Mattigod et al. (2006)
Na	13.1%	12.5%	11.5%	12.0 ± 0.7%	11.7 ± 1.6%
Al	11.5%	11.7%	11.3%	11.5 ± 0.3%	10.7 ± 0.2%
Si	12.0%	11.9%	12.5%	12.2 ± 0.4%	11.6 ± 0.9
Re	26.5%	27.4%	25.8%	26.6 ± 1.1%	30.6 ± 1.2%

[a]Average and standard deviation based on microprobe and chemical digestion analyses.

Bulk Rhenium L_2-edge and Tc K-edge XANES and EXAFS Data. Four reference spectra, Re metal [Re(0)], ReO_2 [Re(IV)], ReO_3 [Re(VI)], and $KReO_4$ [Re(VII)], were used for data fitting, and the spectra collection has been described previously.[3] Data were fit using the locally written program "fites," which performs a non-linear least squares fit of the data (http://lise.lbl.gov/RSXAP). XANES fitting was performed in a series of iterations. The XANES

spectrum of ReO_4^--sodalite initially was fit using all of the reference spectra. If the contribution of any spectrum was smaller than its standard deviation, it was removed from the set of standard spectra, and the fit was repeated. This process was repeated until the contribution of each remaining spectrum was greater than its standard deviation. In the end, only $KReO_4$ contributed to the fit, which used five parameters: the contribution of each standard spectrum, a global energy shift, and a linear correction. Data were fit between 11,940 and 12,040 eV. Data resolution was 5 eV as determined from the Re L_2 white line of measurements performed at the different beam lines, so the XANES spectrum contains 20 independent data points.

EXAFS fitting was performed using Artemis. Theoretical phases and amplitudes were calculated using Feff7 and the structure of nosean with Re replacing S in the sulfate anion (the actual Re-O distance in perrhenate is 0.1 Å shorter than the S-O distance in sulfate).

For technetium three reference spectra, TcO_2 and TcO_4^- absorbed on Reillex HPQ ion exchange resin were used for data fitting. Data were fit using the locally written program "fites," which performs a non-linear least squares fit of the data. Five parameters were used in the fit: the amplitudes of the two standards, one global energy shift, and slope and offset (linear correction to account for differences in normalization). Data were fit between 21,020 and 21,140 eV. Data resolution is estimated to be 7 eV; therefore, there are 17 independent data (spectral range divided by the resolution) in the spectrum.

EXAFS fitting was performed using Artemis. Theoretical phases and amplitudes were calculated using Feff7 and the structure of nosean with Tc replacing S in the sulfate anion (the actual Tc-O distance in pertechnetate is 0.1 Å shorter than the S-O distance in sulfate).

XAFS F-test for Rhenium L_{II}-edge and Technetium K-edge results. The improvement to the fit due to the inclusion of each reference spectrum in the final fit was determined using the F-test.[4] Briefly, the data was fit using the final set of reference spectra to give the best fit. Then, the fit was repeated multiple times with the amplitude of one of the reference spectra set to zero each time, which produced a larger *r*-factor. For each component, *F* was determined using

$$F = \left(\frac{\left(r_q^2 - r_0^2 \right)}{r_0^2} \right) \left(\frac{\left(m - n \right)}{b} \right) \quad (1)$$

where r_q is the *r*-factor of a fit with the amplitude of 1 component set to zero, r_0 is the *r*-factor for the fit including all components, *m* is the number of independent data (16.6), *n* is the number of parameters in the best fit (5), and *b* is the difference between the number of parameters in the best fit and the number of parameters with one component set to zero (1). The probability, *p*, that a given value of *F* was due to random error was determined using Excel.

STEM Imaging. It is important to note that micro- and meso-porous materials can deteriorate rapidly when exposed to 100 kV electron beams. The deterioration of the material is the result of a combination of many factors, such as radiolysis and knock-on damage.[5-7] In the case of perrhenate sodalite, beam damage was readily apparent (Fig. SI2). To minimize beam damage while imaging, the beam dwell time was limited to 2 μs, which resulted in images that were a little noisy due to the short dwell time and relatively low electron dose.

Aberration-corrected HAADF STEM—also referred to as Z-contrast imaging—is a powerful technique for determining the location and distribution of atoms or atomic columns because of the strong dependence on atomic number (Z).[8-11] This is because the intensity of scattered high angle electrons collected at the HAADF detector is proportional to the sample thickness and Z^n,

where *n* ideally gives an intensity of 2, but in practice it ranges from 1.6 to 2. Here the perrhenate sodalite grain is <150 nm thick. For comparison we use *n* = 1.7, which results in Re (Z = 75) in the ReO_4^- anion having a theoretical intensity that is 19.7 and 17.3 times brighter than the framework elements Al (Z = 13) and Si (Z = 14), respectively. It has been shown that STEM at 100 kV accelerating voltage was sufficient to generate a HAADF signal and penetrate thick samples containing elements with medium mass, even when thickness exceeds 100 nm.[12]

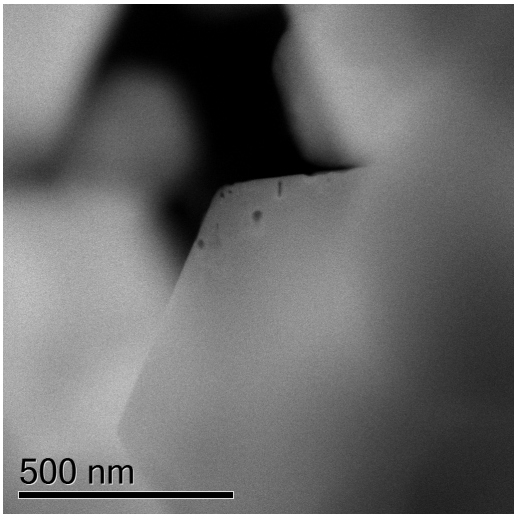

Figure SI2. Aberration-corrected HAADF STEM image showing sample beam damage that occurred to the perrhenate sodalite grain during imaging.

XAFS Analysis and Crystal Structure of Perrhenate Sodalite.

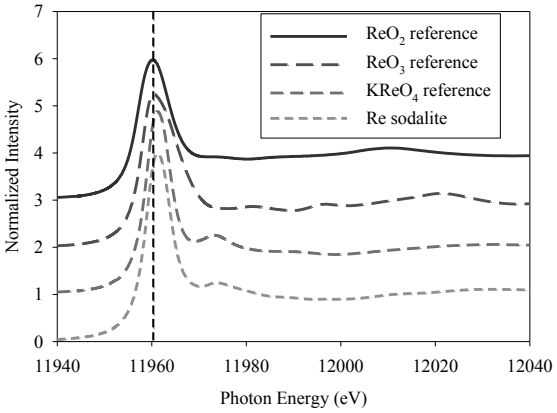

Figure SI3. Re L_2-edge XANES spectra of the three standards used in fitting the XANES spectrum. The perrhenate sodalite sample spectrum is shown for comparison.

Table SI2. Results of XANES spectra fitting of $Na_8[Al_6Si_6O_{24}](ReO_4)_2$

Sample	Beam line	ReO_2	p(F)[a]	ReO_3	p(F)	ReO_4^-	p(F)	*R*-factor[b]
Perrhenate sodalite[c]	APS	0.01(6)	0.86	0.11(4)	0.088	0.81(3)	<0.001	-

[a]p(F) is the probability that the improvement to the fit because of including this component is due to random error. If p(F) < 0.05, the component can be considered to be present.
[b]*r*-factor is $[\Sigma(y_{obs}-y_{calc})^2/\Sigma y_{obs}^2]^{1/2}$, where the sum is over all data.
[c]Data fit using $KReO_4$ as the Re(VII) reference spectra.
[d]Standard deviations of the fitted parameters are given in parentheses as 1σ values.

Table SI3. Results of EXAFS spectra fitting of perrhenate sodalite, $Na_8[AlSiO_4]_6(ReO_4)_2$

Sample	**Beam line**	**Neighbor**	**ΔE_0 (eV)**	**R factor[a]**	**N[b]**	**R[c] (Å)**	**σ^{2d} (Å^2)**
perrhenate sodalite	SSRL& APS	O	6 (2)	0.009	4.0 (5)	1.729 (7)	0.002 (1)

[a]R factor = $[\Sigma(y_{obs}-y_{calc})^2/\Sigma y_{obs}^2]^{1/2}$, where the sum is over all data.
[b]N = Number of neighboring atoms. Meaningless for a fit with one shell. $S_0^2 = 1$ (fixed).
[c]R = Distance to neighboring atoms.
[d]σ^2 = Mean-square disorder of neighbor distance.
[d]Standard deviations of the fitted parameters are given in parentheses as 1σ values.

Table SI4. Atomic positions, site occupancies, and U_{eq} refined from neutron powder diffraction data for perrhenate sodalite, $Na_8[AlSiO_4]_6(ReO_4)_2$

Atom	Label	Site	x	y	z	sof	U_{eq} × 100
Al	Al	6*c*	¼	½	0	1	0.36
Si	Si	6*d*	¼	0	½	1	1.88
O	O1	24*i*	0.1461 (2)	0.1546 (2)	0.4761 (2)	1	2.58
Na	Na	8*e*	0.2383 (4)	0.2383 (4)	0.2383 (4)	1	3.66
Re	Re	2*a*	0	0	0	1	2.86
O	O2	24*i*	0.140 (2)	0.114 (3)	0.007 (1)	0.312 (9)	11.93

Table SI5. Anisotropic atomic displacement parameters (U × 100) refined from the neutron powder diffraction data for perrhenate sodalite, $Na_8[AlSiO_4]_6(ReO_4)_2$

Atom	U_{iso}	U11	U22	U33	U12	U13	U23
Al	0.36 (8)						
Si		2.3 (3)	1.6 (2)	1.6 (2)			
O		2.0 (1)	3.0 (1)	2.77 (9)	1.55 (7)	0.2 (1)	-0.2 (1)
Na		3.7 (1)	3.7 (1)	3.7 (1)	1.5 (1)	1.5 (1)	1.5 (1)
Re		2.86 (7)	2.86 (7)	2.86 (7)	0	0	0
O		8 (1)	13 (1)	15.4 (8)	-8.1 (6)	0 (2)	0 (2)

Errors given in parentheses are 1 σ.

Table SI6. Atomic positions, site occupancies, and U_{eq} refined from the x-ray powder diffraction data for perrhenate sodalite, $Na_8[AlSiO_4]_6(ReO_4)_2$

Atom	Label	Site	x	y	z	sof	U_{eq}
Al	Al	6*c*	¼	½	0	1	0.72 (5)[a]
Si	Si	6*d*	¼	0	½	1	0.72 (5)[a]
O	O1	24*i*	0.1538 (5)	0.1453 (5)	0.4742 (6)	1	1.0 (1)
Na	Na	8*e*	0.2343 (4)	0.2343 (4)	0.2343 (4)	1	2.1(1)
Re	Re	2*a*	0	0	0	1	3.29 (4)
O	O2	24*i*	0.161 (1)	0.097 (1)	0.032 (2)	0.309 (3)	2.0 (6)

[a]Constrained U_{iso} Al = U_{iso} Si.

Errors given in parentheses are 1 σ.

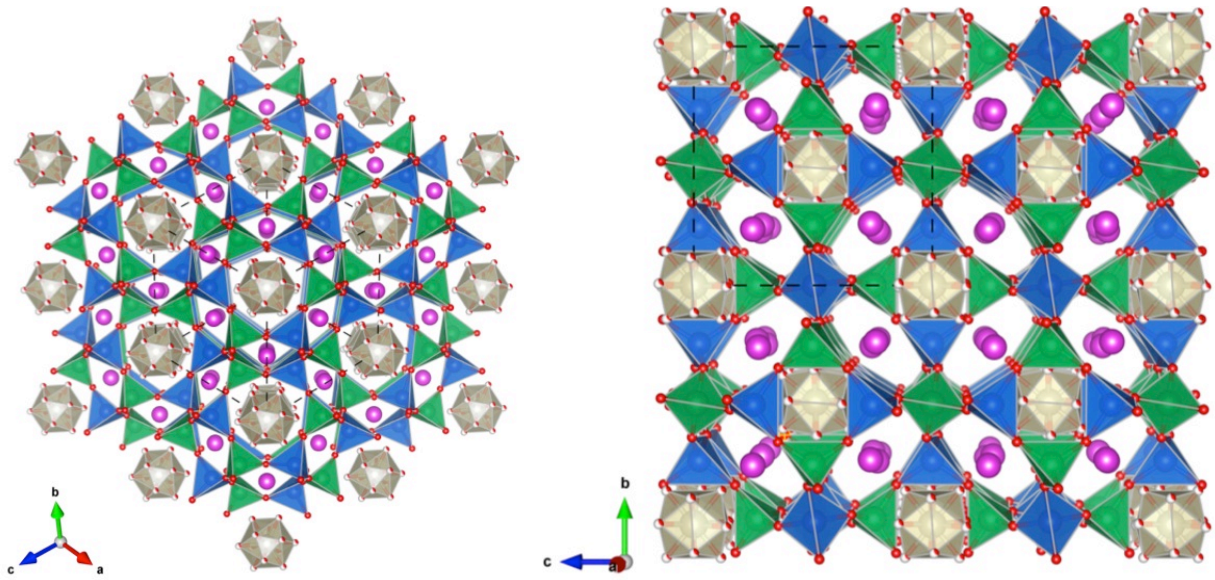

Figure SI4. Structure of $Na_8[AlSiO_4]_6(ReO_{3.75})_2$ drawn along the [111] zone axis (top) and [100] zone axis (bottom) from the refined atomic coordinates given in Table 2, 3, and 4. Sodium is magenta, aluminum is green, silicon is blue, oxygen is red, and rhenium is tan. The 3D visual representation of the crystallographic structure was created with VESTA version 3.3.2.[13]

Selected Area Electron Diffraction. A Focused ion beam (FIB) lift out from a cluster of grains was performed on a Hitachi NB-5000 FIB/SEM. FIB milling was used to prepare an electron transparent perrhenate sodalite sample measuring 25μm × 4 μm × 100nm thick for selected area electron diffraction (SAED). The powdered perrhenate sodalite sample was suspended in IPA and a 100 μL drop cast onto a Si wafer substrate. The Si substrate with perrhenate sodalite agglomerates was imaged with an electron beam until a suitable agglomerate of particles, close the proper orientation for TEM analysis was identified. The FIB preparation, performed with a Hitachi NB5000 FIB/SEM instrument, was achieved by first attaching a perrhenate sodalite particle agglomerate to the micro-manipulation needle with beam deposited carbon. The particle agglomerate was then lifted from the Si substrate and attached to a Cu finger of a Omniprobe half grid and attached to the Cu finger with ion beam deposited W. Thinning to

electron transparency began with deposition of a ~150nm thick W layer onto the particle surface using ion beam deposition (IBID). This W layer is used to reduce "curtaining" during the final FIB thinning of the specimen to electron transparency. After the IBID attachment to the TEM grid was completed a series of milling steps was used to reduce the thickness of the particle until it was electron transparent (~100nm). The thinning was started at with a 40kV, 3.36nA beam and used to thin the sample to ~500nm. The beam current was then reduced to 0.52nA and the sample was thinned to ~250nm. For the final milling step the beam parameters were changed to 20kV, 0.11nA and the sample was thinned to ~100nm thick. To reduce Ga implantation effects and amorphous material on the surface of the FIB thinned sample, a Fischione Nanomill was operated at 900eV to Ar^+ ion mill each side of the sample at 10° for 5min each side.

The FIB sample was used to perform SAED using a 200-kV FEI-Tecnai F20 transmission electron microscope (TEM). SAED was conducted on perrhenate sodalite FIB sample along the [001] zone axis to gain nanometer scale insight on the structure of perrhenate sodalite. A Ted Pella sputtered aluminum diffraction standard was used to calibrate the camera constant, so accurate lattice parameters could be determined from SAED. Fig. SI5 shows the SEM image of the FIB sample, index SAED pattern, and a kinematically SAED simulation conducted with WEBEMAPS [14] along the [001] zone axis. These results reveal a cubic structure with a lattice spacing of 9.14 ±0.04 Å. This lattice spacing is 1% lower than the values measured in the bulk sample and consistent with the lower sensitivity for this technique.

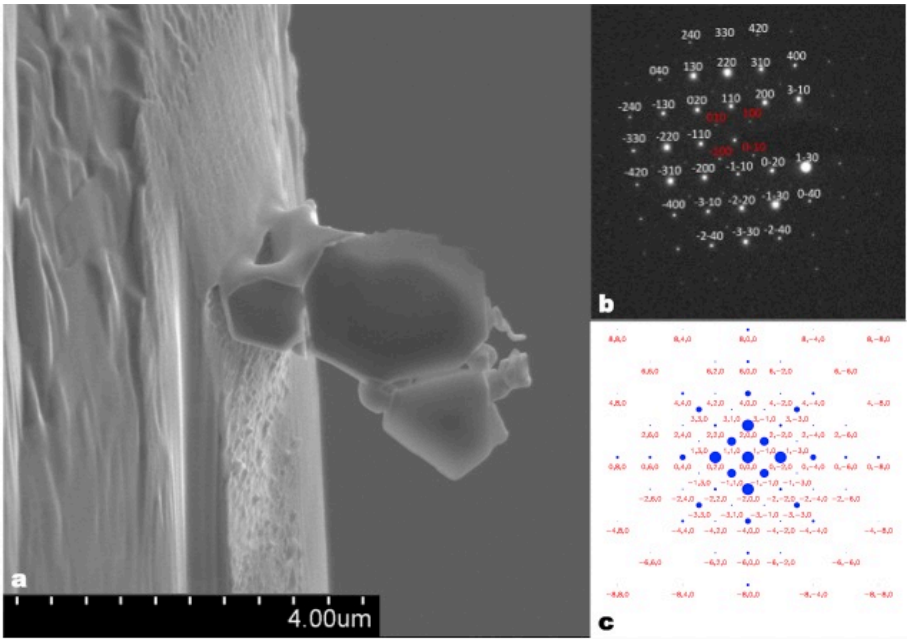

Figure SI5. SEM image of FIB prep perrhenate sodalite sample for selected area electron diffraction (SAED) (a), [001]-zone SAED pattern (b), and a kinematically SAED simulation conducted with WEBEMAPS [14] along the [001] zone axis (c).

Atomic Force Microcopy. Atomic force microscopy (AFM) of perrhenate sodalite was performed with a Bruker Multimode 8 AFM with Nanoscope V controller and an A scanner. The A scanner used in our experiments was calibrated with the conventional Bruker calibration grid and the calibration was checked by collecting high-resolution images of freshly cleaved mica. The perrhenate sodalite sample was deposited on freshly cleaved mica by pipetting 10 μL of a 100 mg/L particle suspension and allowing the sample to dry overnight in a covered dish. The 100 mg/L particle suspension was prepared by adding ~0.20 grams to 6.7-mL of 18 MΩ-cm deionized water (DIW) (~2800 mg/L stock) and diluting the stock solution by pipetting 300 μL of solution into 6.7 mL of DIW. Contact mode AFM images were collected on the [100] and [111] face in air at a scan rate of 24-48 Hz using v-shaped supersharp silicon nitride probes that had a nominal length, spring constant, resonance frequency, and radius of 120 μm, 0.35 N/m, 65

kHz, and 2 nm, respectively. The backside of the probe was coated with gold to increase measurement sensitivity during tip-sample interaction. Scan size varied between 10 × 10 nm and 20 × 20 nm. All images were collected inside an acoustic dampening box that included an elastic cord isolated platform. Collectively this system minimized artifacts caused by external vibrations. All images were flattened using a zero-degree line-wise fit and an average profile global fit using Scanning Probe Image Processor (SPIP^{TM}) software version 6.3.[15]

High resolution AFM images are displayed in Fig. SI6 along with height profiles, lattice spacing, and a 3D visual representation of the [100] and [111] crystal face. The 3D visual representations were created by modeling the [100] and [111] faces of perrhenate sodalite—based on the pXRD and NPD data—and used to aide in image interpretation. The bright spots shown in Fig. SI6a correspond to the sodalite β-cages with the upper most ReO_4^- anion absent from the surface. This is supported by the measured depth between the bright spots on the [100] face of ~0.4 nm, as seen in the cross-section below (Fig. SI6a). Taking into consideration the finite shape of the tip we measured from the center of the upper most oxygen plane to the center of the sodium plane on the [100] crystal face resulting in a depth of 0.37 nm. This value is in good agreement with the measured depth. The bright spots on the [111] face (Fig. SI6b) also correspond to the sodalite β-cages with a depth of ~0.25 nm, see the cross section below Fig. SI6b. The depth measured from the center of the upper most Na plane to the center of the middle Na plane of in our model on the [111] face resulted in a distance of 0.24 nm further supporting the absence of the ReO_4^- anion on the surface of the sodalite. Insets of the modeled surfaces are shown in Fig. SI6 where oxygen is shown in red and sodium is shown in purple.

The lattice distances of the [100] face are also shown in Fig. SI6a. The measured [100] lattice distances are averages taken from 12 images. The calculated lattice distance for the [100] crystal

face is 0.915 nm. These distances are in good agreement with the crystal structure within experimental error. The lattice distances of the [111] crystal face along the fast scan axis (left to right) are shown in Fig. SI6b. The measured [111] lattice distances are averages taken from 23 images. The calculated lattice distance for the [111] face is 1.29 nm. The average of the two lattice vectors results in a spacing of 1.30 nm in good agreement with the crystal structure and is within experimental error. The lattice distance along the slow axis (top to bottom) results in a lattice spacing of 1.60 ± 0.18 nm, which is significantly larger than the expected lattice distance of 1.29 nm. This difference is attributed to drift in the scanner while imaging and is expected to have a greater impact on the measured distances in the slow scan direction as observed.

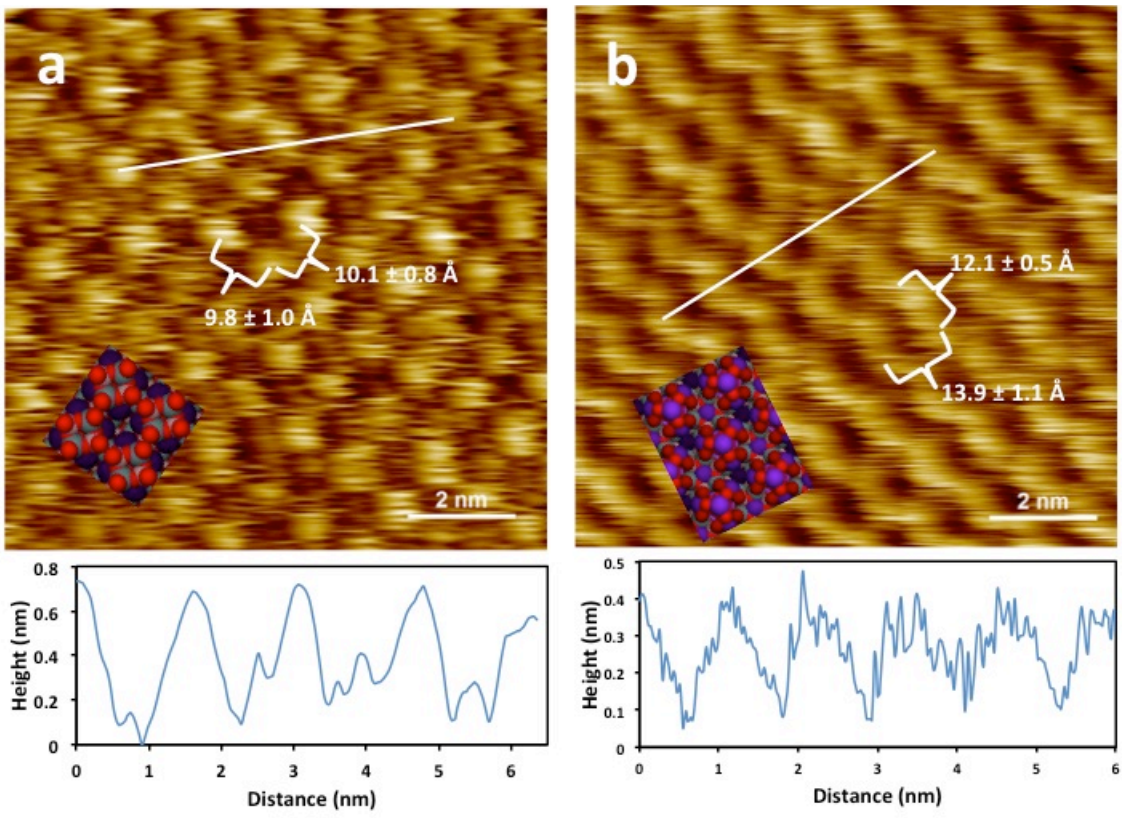

Figure SI6. Surface topography image along the [100] face (left) and [111] face (right).

XAFS and Crystal Structure of Mixed Perrhenate/Pertechnetate Sodalite.

Table SI7. Results of EXAFS spectra fitting of mixed guest perrhenate/pertechnetate sodalite, $Na_8[AlSiO_4]_6(ReO4)_{2-x}(TcO_4)_x$

Sample	Beam line	Neighbor	Number of Neighbors	Distance (Å)	σ^2 (Å^2)
mixed guest sodalite	*NSLS X27A*	*O*	4.5(6)	1.722 (5)	0.002 (1)

$S_0^2 = 1$ (fixed), $\Delta E_0 = -18(3)$ eV
Standard deviations of the fitted parameters are given in parentheses as 1 σ values.

Table SI8. The atomic positions, site occupancies, U_{eq} refined from the x-ray powder diffraction data collected on $Na_8[AlSiO_4]_6(ReO_4)_{2-x}(TcO_4)_x$

Atom	**Label**	**Site**	**x**	**y**	**z**	**sof**	**U_{eq} × 100**
Al	Al	6*c*	¼	½	0	1	2.8 (6)
Si	Si	6*d*	¼	0	½	1	1.5 (6)
O	O1	24*i*	0.153 (1)	0.147 (1)	0.471 (1)	1	2.5
Na	Na	8*e*	0.2328 (8)	0.2328 (8)	0.2328 (8)	1	2.7 (3)
Re	Re	2*a*	0	0	0	0.74 (2)	3.6 (2)
Tc	Tc	2*a*	0	0	0	0.26 (2)	3.6 (2)
O	O2	24*i*	0.161 (1)	0.097 (1)	0.032 (2)	0.309 (3)	2.0 (6)

Errors given in parentheses are 1 σ.

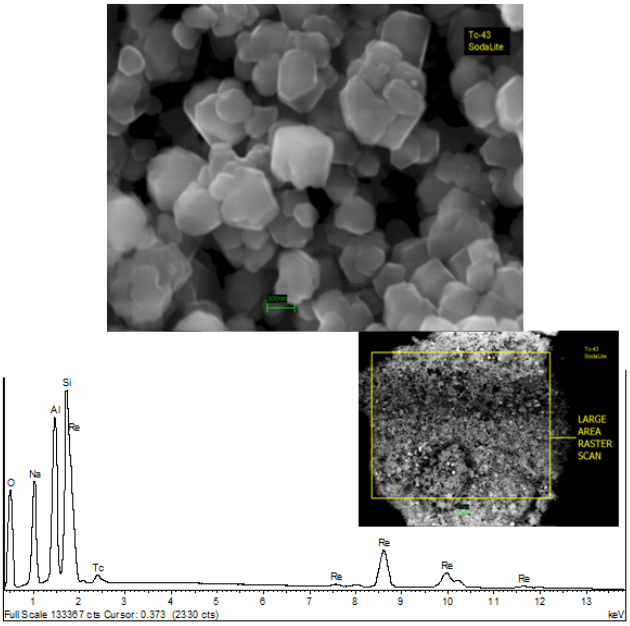

Fig. SI7. Scanning electron microscope image and energy dispersive spectroscopy analysis of the $Na_8[AlSiO_4]_6(ReO_4)_{1.48}(TcO_4)_{0.52}$ sample.

Thermogravimetric and Heat Capacity measurements. Two types of thermogravimetric measurements were performed at 1,073 and 1,273 K. The first type of TG measurements consisted of annealing a sodium perrhenate salt ($NaReO_4$) in an empty Pt crucible at 1,273 K, whereas the second represented dissolving the perrhenate sodalite in molten lead borate at 1,073 K. In both cases, the initial and final weights were measured to determine any weight loss related to the water content or other possible reactions. Annealing dry perrhenate sodalite at 1,073 K and above results in a partial decomposition of the sample. The XRD results of the final $NaReO_4$ product of annealing in an empty Pt crucible showed that no structural changes occurred.

To verify the thermogravimetric procedure in molten lead borate at 1,073 K, additional experiments were performed. A sodium natrolite zeolite ($Na_{0.382}Al_{0.402}Si_{0.603}O_2 \bullet 0.47H_2O$) with known water content was dissolved in lead borate, and the weight change was measured. The obtained value was consistent within the experimental error with that previously measured by

TG/DSC, using a Setaram Labsys Evo instrument.[1] As a final crosscheck, the calorimetric results for dehydrated and corrected for water content nosean samples ($Na_{7.98}Al_{6.00}Si_{6.06}S_{1.02}O_{28}$•$2.79H_2O$) were compared and found to be consistent within the experimental errors [see manuscript in preparation]. No structural or adsorbed water was found in the perrhenate sodalite, which is consistent with the FTIR measurements.

A separate study of the heat capacity of perrhenate sodalite and sodium perrhenate will be published, providing all the data from 2 to 300 K, as well as the calculated thermodynamic functions.

Table SI9. Thermodynamic cycles used to calculate the enthalpy of formation for the compound $Na_8[AlSiO_4]_6(ReO_4)_2$, from components and from elements

Reaction number and reaction	**Enthalpy of the reaction (kJ/mol)**
$Na_8\left[AlSiO_4\right]_6\left(ReO_4\right)_2\left(s,298.15K\right) \rightarrow 3Na_2O\left(soln,973K\right)+2NaReO_4\left(soln,973K\right)$ $+3Al_2O_3\left(soln,973K\right)+6SiO_2\left(soln,973K\right)$	ΔH_1
$Na_2O\left(s,298.15K\right) \rightarrow Na_2O\left(soln,973K\right)$	ΔH_2
α-$Al_2O_3\left(s,298.15K\right) \rightarrow Al_2O_3\left(soln,973K\right)$	ΔH_3
$SiO_2\left(s,298.15K\right) \rightarrow SiO_2\left(soln,973K\right)$	ΔH_4
$NaReO_4\left(s,298.15K\right) \rightarrow NaReO_4\left(soln,973K\right)$	ΔH_5
$3Na_2O\left(s,298.15K\right)+2NaReO_4\left(s,298.15K\right)+3Al_2O_3\left(s,298.15K\right)+6SiO_2\left(s,298.15K\right)$ $\rightarrow Na_8[AlSiO_4]_6(ReO_4)_2\left(s,298.15K\right)$	ΔH_6
$\Delta H_6 = \Delta H_{f,ox} = -\Delta H_1 + (a-x)\Delta H_2 + b/2\Delta H_3 + c\Delta H_4 + x\Delta H_5$	

Table SI10. Thermodynamic cycles used to calculate the enthalpy of formation of a compound $Na_aAl_bSi_cX_xO_{24}$ where X is SO_4, CO_3, NO_3, ReO_4, from components. The numerical values are shown in Table S5.

Reaction number and reaction	**ΔH_r (kJ/mol)**
$Na_aAl_bSi_cX_xO_{24}$ (s, 298 K) → (a–x)Na_2O (soln, 973K) + xNaX (soln, 973K) + b/2Al_2O_3(soln, 973K) + cSiO_2 (soln, 973K)	ΔH_1
Na_2O (s, 298 K) → Na_2O (soln, 973K)	ΔH_2
α–Al_2O_3 (s, 298 K) → Al_2O_3 (soln, 973K)	ΔH_3
SiO_2 (s, 298 K) → SiO_2 (soln, 973K)	ΔH_4
NaX (s, 298 K) → NaX (soln, 973 K)	ΔH_5
(a+c)Na_2O (s, 298 K) + xNaX(s, 298 K) + b/2Al_2O_3(s, 298 K) + cSiO_2 (s, 298 K) → $Na_8Al_6Si_6X_xO_{24}$ (s, 298 K)	ΔH_6
$\Delta H_6 = \Delta H_{f,ox} = -\Delta H_1 + (a-x)\Delta H_2 + b/2\Delta H_3 + c\Delta H_4 + x\Delta H_5$	

Table SI11. The enthalpies and entropies of formation of the sodalites and cancrinites, standard entropies of all compounds, and the Gibbs free energy of formation

Compound	**$\Delta H_{f,comp}$, kJ/mol**	**S_{298}, J/mol.K**	**$\Delta S_{f,comp}$, J/mol.K**	**$\Delta G_{f,comp}$, kJ/mol**	**Reference**
Nosean, $Na_8[AlSiO_4]_6(SO_4)$	-718.68 ± 8.76	986.41	261.01	-796.46	This work
Perrhenate sodalite, $Na_8[AlSiO_4]_6(ReO_4)_2$	-814.02 ± 10.68	1149.10	217.47	-878.82	This work
Nitrate cancrinite, $Na_8[Al_{0.975}Si_{1.025}O_4)]_6(NO_3)_2$	-795.46 ± 9.75	1000.00	220.13	-861.06	Liu et al. [16]
Carbonate cancrinite, $Na_8[AlSiO_4)]_6(CO_3)$	-684.37 ± 18.92	985.95	272.14	-765.47	Kurdakova et al., [17]
Na_2O		75.04			JANAF[a]
α–Al_2O_3		50.95			JANAF
SiO_2		41.46			JANAF
$NaReO_4$		152.43			This work
Na_2SO_4		149.60			JANAF
Na_2CO_3		138.80			JANAF
$NaNO_3$		116.00			JANAF

[a]JANAF = Joint-Army-Navy-Air Force Thermochemical Tables project.
All errors reported are 2σ (i.e., 2 standard deviations from the mean)

Table SI12. Ionic radii and potential of the oxyanion.

Oxyanion	Ionic radius, Å	Ionic potential, Å	Reference
SO_4^{2-}	2.3	0.870	Gloe et al. [18]
ReO_4^-	2.6	0.385	
NO_3^-	1.79	0.559	
CO_3^-	1.78	1.124	
TcO_4^-	2.52	0.397	

REFERENCES

1. Wu, L. L.; Navrotsky, A.; Lee, Y. Thermodynamic study of alkali and alkaline-earth cation-exchanged natrolites. *Microporous and Mesoporous Materials* **2013,** *167*, 221–227.
2. Mattigod, S. V.; McGrail, B. P.; McCready, D. E.; Wang, L.; Parker, K. E.; Young, J. S. Synthesis and structure of perrhenate sodalite. *Microporous and Mesoporous Materials* **2006,** *91* (1-3), 139-144.
3. Lukens, W. Dissimilar behavior of technetium and rhenium in borosilicate waste glass as determined by x-ray absorption spectroscopy. *Chemical Material* **2007,** *19*, 559.
4. Downward, L.; Booth, C. H.; Lukens, W. W.; Bridges, F. In *A Variation of the F-Test for Determining Statistical Relevance of Particular Parameters in EXAFS Fits*, AIP Conference, American Institute of Physics: 2007; pp 129-131.
5. Treacy, M. M. J.; Newsam, J. M. Electron beam sensitivity of zeolite L. *Ultramicroscopy* **1987,** *23*, 411.
6. Bursill, L. A.; Lodge, E. A.; Thomas, J. M. Zeolitic structures as revealed by high-resolution electron microscopy. *Nature* **1980,** *286*, 111.
7. Yokota, Y.; Hashimoto, H.; Yamaguchi, T. Electron-beam irradiation of natural zeolites at low and room temperatures. *Ultramicroscopy* **1994,** *54* (2-4), 207-214.
8. Muller, D. Structure and Bonding at the atomic scale by scanning transmission electron microscopy. *Nature Materials* **2009,** *8*, 263-270.
9. Voyles, P.; Muller, D.; Grazul, J.; Citrin, P.; Gossmann, H.-J. Atomic-scale imaging of individual dopant atoms and clusters in highly n-type bulk Si. *Nature* **2002,** *416*, 826-829.
10. Buban, J.; Matsunaga, K.; Chen, J.; Shibata, N.; Ching, W.; Yamamoto, T.; Ikuhara, Y. Grain boundary strengthening in alumina by rare earth impurities. *Science* **2006,** *311*, 212-215.
11. Pennycook, S.; Nellist, P., Scanning Transmission Electron Microscopy Imaging and Analysis. Springer: New York, 2011; pp 20-36.
12. LeBeau, J.; Findlay, S.; Allen, L.; Stemmer, S. Quantitative atomic resolution scanning transmission electron microscopy. *Physical Review Letters* **2008,** *100*, 206101.
13. Momma, K.; Izumi, F. VESTA 3 for three-dimensional visualization of crystal, volumetric and morphology data. *Journal of Applied Crystallography* **2011,** *44*, 1272-1276.
14. Zuo, J. M.; Mabon, J. C. Web-based Electron Microscopy Application Software: Web-EMAPS. *Microscopy and Microanalysis* **2004,** *10*.

15. Metrology, I. *The Scanning Probe Image Processor: SPIP User's and Reference Guide*., 6.3; Denmark, 2014.
16. Liu, Q.; Navrotsky, A.; Jove-Colon, C.; Bonhomme, F. Energetics of cancrinite: Effect of salt inclusion. *Microporous and Mesoporous Materials* **2007,** *98*, 227–233.
17. Kurdakova, S.; Grishchenko, R.; Druzhinina, A.; Ogorodova, L. Thermodynamic properties of syntethic calcium-free carbonate cancrinite. *Phys. Chem. Miner.* **2013,** *41*, 75–83.
18. Gloe, K.; Stephan, H.; Grotjahn, M. Where is the anion extraction going? *Chemical Engineering & Technology* **2003,** *26* (11), 1107–1117.